Available online at www.sciencedirect.com

ScienceDirect

Procedia Engineering 2 (2010) 1005–1014

Procedia Engineering

www.elsevier.com/locate/procedia

Fatigue 2010

An analytical model of plasticity induced crack closure

F. V. Antunes[a,]*, D. M. Rodrigues[a], R. Branco[b]

[a]*CEMUC, Department of Mech Eng, University of Coimbra, Rua Luís Reis Santos, Pinhal de Marrocos, 3030-788 Coimbra, Portugal*
[b]*Department of Mech Eng, Polytechnic Institute of Coimbra, Rua Pedro Nunes, Quinta da Nora, 3030 - 129 Coimbra, Portugal*

Received 27 February 2010; revised 12 March 2010; accepted 15 March 2010

Abstract

Accurate and non-conservative measurements of fatigue crack growth rate are essential when designing efficient structures to be subjected to cyclic loading. Crack closure is a main mechanism of fatigue crack propagation and must be included. Numerical models have been successfully developed to predict plasticity induced crack closure (PICC), however a full understanding of the links between physical parameters, residual plastic wake and PICC has not been achieved yet. The objective of the present paper is the identification of the main micromechanisms involved in PICC and the establishment of qualitative and quantitative links between plastic deformation and the level of PICC. An M(T) specimen with 200×60×0.2 mm^3 and an initial crack of 10 mm was studied. It was found that the linear superposition applies to the effect of individual plastic wedges on the PICC level. The vertical elongation of the plastic wedge, Δy, was considered and found adequate to quantify the weight of individual plastic wedges in the residual plastic wake. The effect of an individual plastic wedge was found to have an exponential decrease with the distance to the crack tip, d. An empirical model was developed relating the PICC level of individual plastic wedges with the distance d and the plastic deformation level, Δy, and was applied successfully to predict PICC evolution from residual plastic wakes.

Keywords: Plasticity induced crack closure; finite element method; micromechanisms; residual plastic wake

1. Introduction

Accurate and non-conservative measurements of FCGR are essential when designing efficient structures subject to cyclic loading. One cause of conservatism in FCGR prediction has been the neglect of the crack closure phenomenon, which consists of the contact of the fracture surfaces during a portion of the load cycle, and is usually associated with plastic deformation, oxide particles or roughness at the crack flanks [1–3]. This contact affects the local stress and plastic deformation fields near the crack tip, and therefore the micromechanisms responsible for fatigue propagation. Current applications of fracture mechanics concepts to fatigue crack advance characterization are generally based on the premise that the compression portion of a fatigue cycle does not contribute to the growth of fatigue cracks. Crack closure seems to be able to explain the influence of mean stress in both regimes I and II of crack propagation [4,5], the transient crack growth behavior following overloads [6], and the effect of thickness

* Corresponding author.
E-mail address: fernando.ventura@dem.uc.pt.

1877-7058
doi:10.1016/j.proeng.2010.03.109

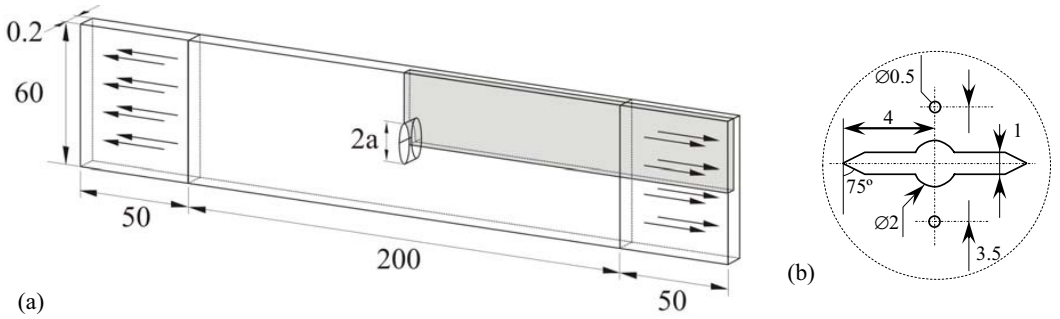

Fig. 1. (a) Middle-tension M(T) specimen. (b) Details of the initial notch.

[7,8], among other aspects. So, crack closure is an extrinsic mechanism affecting the intrinsic damage mechanisms and the fatigue crack growth rate (FCGR), and must be considered in the design of components.

According to Elber's understanding of crack closure [4,9], as the crack propagates due to cyclic loading, a residual plastic wake is formed. The deformed material acts as a wedge behind the crack tip promoting the contact of fracture surfaces during recovery of the surrounding elastically deformed material. Numerical models have been successfully developed to predict PICC and to understand the basic micromechanisms associated with it [10]. Most of these studies focused on the optimization of the large number of numerical parameters [11,12], and on the influence of physical parameters such as crack shape, stress state, or variable amplitude loading [13,14]. However, a full understanding of the links between physical parameters, the strain field and PICC has not been achieved yet.

The generation of a residual plastic wake and its relation with load and material parameters has been studied qualitatively. It was found that the plastic deformation level depends mainly on monotonous and reversed plastic deformation happening at current crack tip, but also on cyclic deformation mechanisms (strain ratcheting, mean stress relaxation and cyclic hardening or softening). The increase of the size of the forward plastic zone, which is constituted by the material near the crack tip undergoing plastic deformation at the maximum load, is expected to increase the level of plasticity induced crack closure (PICC). The monotonous plastic deformation field is enlarged by the increase of the load or/and crack length (i.e., by the increase of K_{max}) and by plane stress conditions (instead of plane strain). The size of the reversed plastic zone, which is formed by the material near the crack tip undergoing compressive yielding at minimum load, is influenced by ΔK, stress state and material behavior. In materials with significant Bauschinger effect, important deformation occurs during unloading, reducing closure level and compressive residual stresses ahead of the crack tip. Accordingly, the use of pure kinematic hardening models was found to produce the largest reversed plastic zone, while the pure isotropic models were found to produce the smallest zones [15]. The sizes of the monotonous and reversed plastic zones have been used to define the size of finite element meshes and the crack propagation needed for stabilization. According to Solancki *et al.* [16], there must be 3-4 linear elements within the reversed plastic zone, while Roychowdhury *et al.* [17] suggested 2-3 linear elements. The crack propagation required for stabilization, Δa_{stb}, is usually defined as a fraction of the size of the monotonic plastic zone resulting from the first load cycle. Values of half [18], one [19,20], two [16] and four [21] have been reported for , Δa_{stb} under plane stress conditions. Under plane strain conditions, values of one [16], four [22,23] and eight [24] have been suggested. An explanation for these differences has not been proposed.

The objective of present paper is the identification of the main micromechanisms explaining PICC and the establishment of qualitative and quantitative links between residual plastic deformation and the level of PICC. This is expected to be a step towards physically based models of PICC. The numerical analysis based on the finite element method was the tool selected. Material properties and load parameters have been manipulated to isolate and understand phenomena.

2. Numerical procedure

Figure 1 illustrates the geometry of the Middle-Tension (M(T)) specimens studied here, which is in agreement with ASTM E647 standard. An initial crack length a_0=5 mm was modelled. Figure 2 shows the physical model

Table 1. Load level in constant amplitude tests

Load	F_{min} [N]	F_{max} [N]	σ_{max} [MPa]	σ_{max}/σ_{ys}
1	0	60	20	0.16
2	0	80	26.7	0.22
3	0	100	33.3	0.27
4	0	140	46.7	0.38
5	0	180	60	0.48
6	0	200	66.7	0.54
7	0	220	73.3	0.59

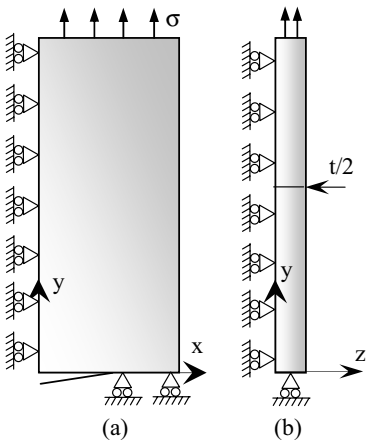

Fig. 2. Boundary conditions (t/2=0.1 mm).

assumed in the numerical analysis. Due to the symmetry of the sample and of loading conditions, only 1/8 of the MT specimen was simulated, by using adequate boundary conditions (Fig. 2). The opposite crack surface was simulated by assuming frictionless contact conditions over a symmetry plane placed behind the growing crack front. The thickness of the model is $t/2 = 0.1$ mm, therefore the total thickness of the specimen is $t = 0.2$ mm.

Different loading conditions were considered, namely, constant amplitude loading and single overload. In the constant amplitude tests, the model of figure 2 was submitted to the loads presented in table 1. An overload ratio was defined as

$$\mathrm{OLR} = \frac{\sigma_{ol} - \sigma_{min}}{\sigma_{max} - \sigma_{min}} \qquad (1)$$

where σ_{min}, σ_{max} and σ_{ol}, are the minimum, maximum and overload stresses, respectively.

The material parameters used in the numerical simulations corresponded to the 6016-T4 aluminium alloy (92 HV0.5). In order to characterize the hardening behaviour of this aluminium alloy, three types of mechanical tests were performed: uniaxial tensile tests and monotonic and Bauschinger shear tests. From the experimental data and curve fitting results [25], for different constitutive models, it was determined that the mechanical behaviour of this alloy is accurately modelled using a Voce type equation

$$Y = Y_0 + R_{sat}(1 - e^{-n_v \bar{\varepsilon}^p}) \ , \qquad (2)$$

to describe the isotropic component of hardening, combined with the saturation law

$$\dot{X} = C_x \left[X_{sat} \frac{(\sigma' - X)}{\overline{\sigma}} - X \right] \dot{\overline{\varepsilon}}^p, \tag{3}$$

to describe the kinematic component of hardening. In these equations Y is the equivalent flow stress, $\overline{\varepsilon}^p$ is the equivalent plastic strain, Y_0 is the initial yield stress, R_{sat} is the saturation stress, n_v, C_x and X_{sat} are material constants, $\boldsymbol{\sigma}'$ is the deviatoric stress tensor, X is the back stress tensor, $\dot{\overline{\varepsilon}}^p$ the equivalent plastic strain rate and $\overline{\sigma}$ the equivalent stress. The material constants used in the numerical simulations were: Y_0=124 MPa, R_{sat}=291 MPa, n_v= 9.5, C_x= 146.5 and X_{sat}= 34.90 MPa.

Figure 3 presents the finite element mesh, which was refined at the crack front, to enable the numerical simulation of the severe plastic deformation gradients, and enlarged at remote positions, to reduce the numerical effort. The radial size considered for the elements around the crack front was L_1=16 μm and the total number of linear isoparametric elements and nodes were 2587 and 5382, respectively. To overcome convergence difficulties, crack propagation was simulated by successive debonding of nodes at minimum load. Each crack increment (Δa_i) corresponded to one finite element and two load cycles were applied between increments. In each cycle, the crack propagated uniformly over the thickness by releasing both crack front nodes. Crack extensions of 0.96 mm were simulated, which correspond to 60 crack propagations. The opening load, F_{op}, was determined by evaluating the contact status of the first nodes behind current crack tip with the symmetry plane. Considering the discrete character of the finite element simulations, the exact opening load was obtained from the linear extrapolation of the loads corresponding to the two increments following opening.

The numerical simulations were performed with a three-dimensional elastic-plastic finite element program (DD3IMP) that follows a fully implicit time integration scheme [26,27]. The mechanical model and the numerical methods used in the finite element code, specially developed for the numerical simulation of metal forming processes, takes into account the large elastic-plastic strains and rotations occurring during large deformation processes. To avoid the locking effect, a selective reduced integration scheme was used [28,29]. The optimum values for the numerical parameters of the DD3IMP implicit algorithm had been already established in previous works, concerning the numerical simulation of sheet metal forming processes [30] and PICC [31].

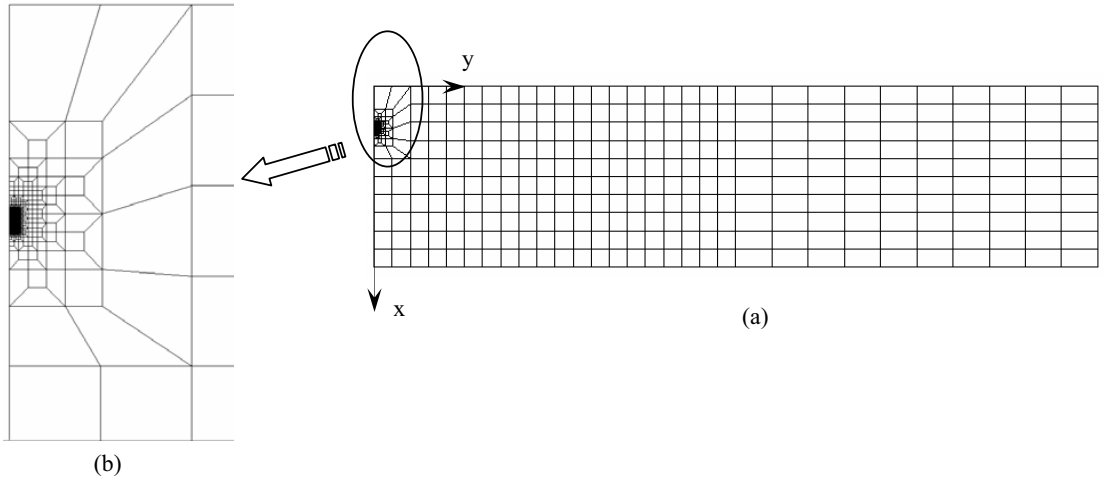

Fig. 3. Finite element mesh. (a) Frontal view. (b) Detail of frontal view.

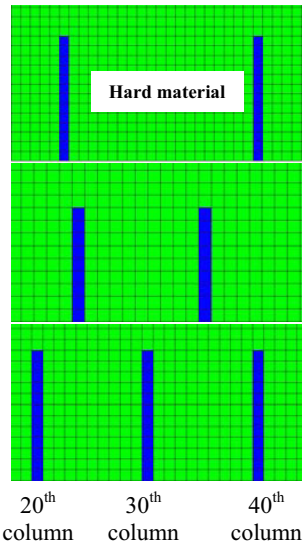

Fig. 4. Individual residual plastic wedges.

3. Numerical results

3.1. Linear superposition principle

In present work, some samples with manipulated material properties were created, as exemplified in Fig. 4, to check if the linear superposition principle applies to the effect of residual plastic wedges on PICC. More precisely, finite element models were generated in which soft material strips, having the material properties of the 6016-T4 aluminum alloy, and embedded in a surrounding hard material matrix simulated by increasing artificially the yield stress of the alloy (Y_0 = 9524 MPa in Eq. (2)). The choice of the yield stress for the hard matrix was performed in order to insure that plastic deformation during cyclic loading was restricted to the soft material columns, distributed along the crack flanks and simulating individualized plastic wedges. The different plastic wedges were identified according to its location relative to the initial crack tip position (20^{th}, 30^{th} and 40^{th} columns). It was found that the effect of 20^{th} column on the closure measured at the 40th column (Fig. 4a), plus the effect of 30th column (Fig. 4b), was nearly equal to the effect of both columns simultaneously (Fig. 4c), with a difference of only about 0.5%. This study was repeated for different number and locations of the individualized plastic wedges along the hardened crack flank, always with the same positive results. Therefore, it was concluded that the linear superposition effect applies to the effect of individual plastic wedges on PICC level.

3.2. Effect of distance to crack tip

Figure 5a shows the contribution of individual plastic wedges to the level of PICC, versus their distance to the crack tip, *d*. Constant amplitude crack propagation tests were considered to define the curves represented. Notice that, as is illustrated in Fig. 5b, crack propagation adds plastic wedges at the crack tip. Analyzing the situation from the point of view of the crack tip, for each crack propagation a plastic wedge is added at the most remote position along crack flank. The corresponding variation of the global PICC is the effect of this "new" plastic wedge at a distance *d*. As shown in Figure 5a, the effect of an individual plastic wedge on PICC decreases strongly with increasing distance (*d*) to the crack tip. Increasing the load level increases the influence of the individual plastic wedges, as could be expected. Assuming that the influence of plastic wedges can be neglected when the variation of

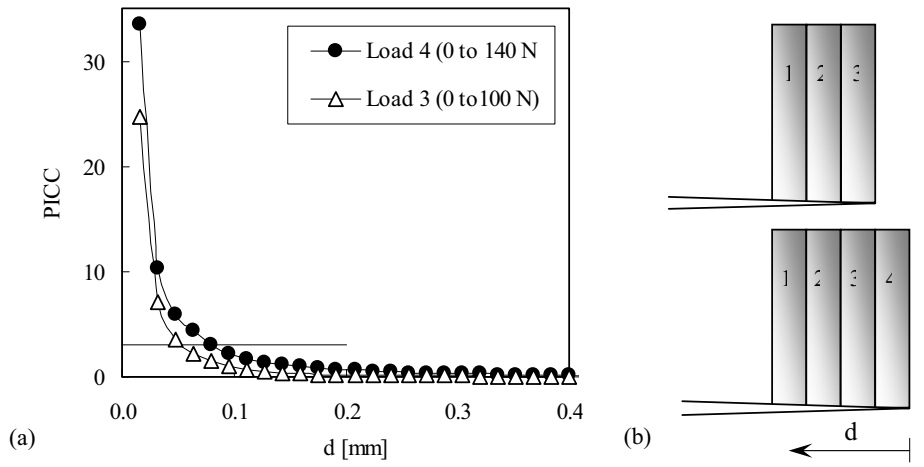

Fig. 5. (a) PICC variation versus distance to crack tip, *d*, in constant amplitude tests. (b) Formation of residual plastic wake in constant amplitude crack growth.

PICC reduces above a particular limit, defined in Fig. 5a by the horizontal line, it is possible to see that the extension of the influence increases with load level, i.e., with plastic deformation level.

3.3. Effect of plastic deformation level

In order to quantify the influence of the plastic deformation on PICC, a global parameter able to characterize the plastic wedge is required. In present work, the integration of the strain normal to the crack flank (ε_{yy}) versus y curve, was considered:

$$\Delta y = \int_0^h \varepsilon_{yy}.dy \qquad (4)$$

which represents the vertical elongation of the plastic wedge. Figure 6a shows the distribution of ε_{yy}, after crack propagation, for load case 4 (F_{min}= 0, F_{max}=140). According to the figure, the finite elements at the first crack tip position have the highest plastic deformation levels, which results from the hardening of the initially non-plastically deformed material at the beginning of crack propagation. Following the initial crack tip strain field, there is a relatively large region with stabilized strain values, which ends at the final position of crack tip. Figure 6b shows the variation of Δy with x-coordinate and with load level. In the graph, the vertical lines represent the beginning and end of crack propagation. For relatively low load levels, at the beginning of crack propagation, Δy has a relatively low value, although the peak of plastic deformation observed in figure 6a. In fact, Δy represents the integration over a height h = 0.3 mm, and although one or two elements at the initial crack tip have relatively large deformation, the global value is small because the deformation in the region ahead is small. In fact, the plastic deformation region ahead of crack tip has a slope of about 70º, therefore the region corresponding to 90º has relatively low deformation. However, for load case 5 (F_{min}= 0, F_{max}=180), the strong deformation near the horizontal symmetry plane is enough to produce a peak of Δy at the beginning of crack propagation. In the intermediate region, Δy has nearly stabilised values, while on the right end side of the curve (i.e., for relatively large values of x), Δy has a sudden drop ahead of the last crack tip position. The increase in load level produces a quite large increase in Δy, as could be expected.

Figure 7 shows the variation of PICC with Δy, for fixed values of the distance, d, to the crack tip. According to the graph, there is a strong increase of PICC with Δy, for relatively low values of this, while for relatively large values of Δy the PICC levels tend to stabilize.

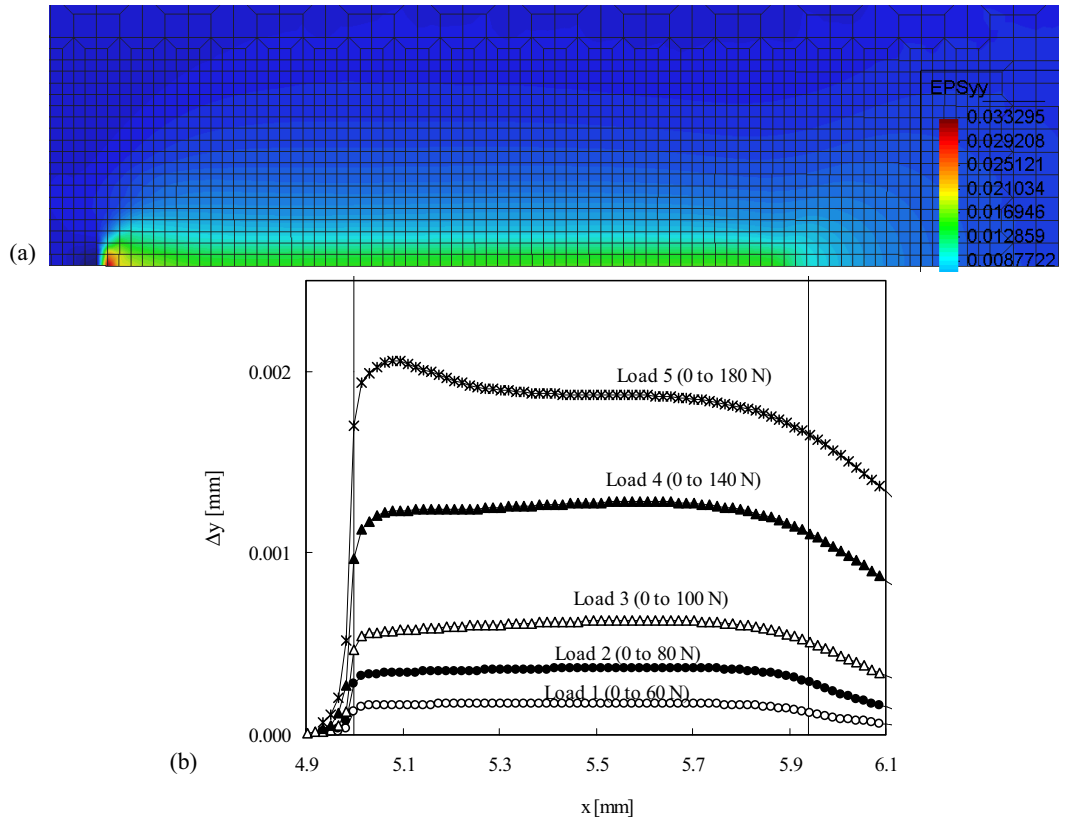

Fig. 6. (a) Strain field (ε_{yy}) for load case 4 (F_{min}= 0, F_{max}= 140). (b) Variation of Δy with x-coordinate and with load level.

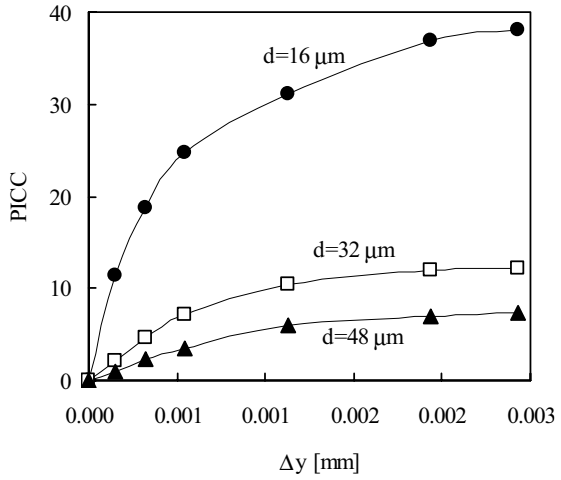

Fig. 7. PICC vs. Δy of individual plastic wedges at different distances to the crack tip.

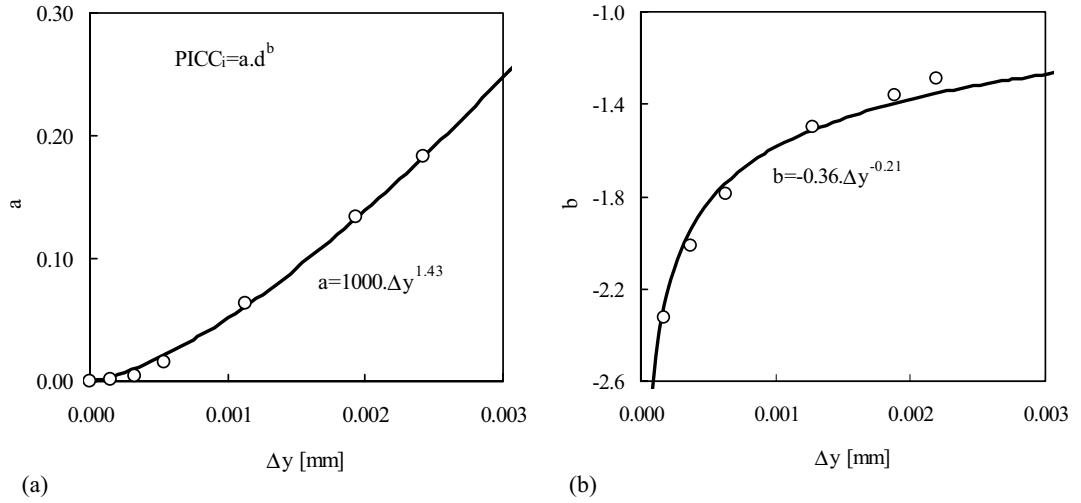

Fig. 8. Evolution of the *a* and *b* constants of eq. (6).

3.4. Analytical model

An analytical model was developed, based on previous results. The basic idea is to establish a relation between an individual plastic wedge, characterized by its position (d) and magnitude (Δy), and the level of PICC. An excellent fitting was found with the exponential model

$$\mathrm{PICC}_i = \tilde{f}(\mathrm{d}, \Delta y) = a \cdot \mathrm{d}^b \qquad (6)$$

where *a* and *b* are fitting constants dependent on Δy. Figures 8a and 8b show the evolution of *a* and *b* constants of eq. (6) with Δy, respectively. As indicated in the figure, a good fitting was found with exponential models, but better results were found with polynomial models. It is important to notice that, since there is a huge sensitivity of PICC previsions to relatively to the *a* and *b* parameters, accurate models are fundamental. In the analytical model, the global level of PICC produced by a residual plastic wake is obtained by summing the effects of all individual plastic wedges (PICC_i) behind crack tip, which are given by eq. (6).

The model was applied to the analysis of different situations, including variable amplitude loading. Figure 9 shows the results obtained with the application of an overload of 160 N after a crack extension of 0.369 mm (baseline loading: F_{min}= 0, F_{max}= 140 N). In Figure 9a, where the ε_{yy} strain field is shown, the plastic deformation produced by the overload is evident. This plastic deformation produces a strong increase of Δy, as Fig. 9b illustrates. Finally, Fig. 9c compares the PICC results obtained from the finite element method with those calculated using the analytical model of eq. (6). The excellent agreement between the curves validates the analytical model and the methodology followed to deduce it. In fact, the model is interesting because isolates the effect of residual plastic wedges, from other phenomena, like discontinuous closure or crack tip blunting.

4. Conclusions

A numerical model based on finite element method was developed to predict plasticity induced crack closure (PICC). In the model, the material properties and the applied loads were manipulated in order to isolate basic micromechanisms of crack closure and to develop qualitative and quantitative relations between individual plastic wedges and PICC. The main conclusions are:

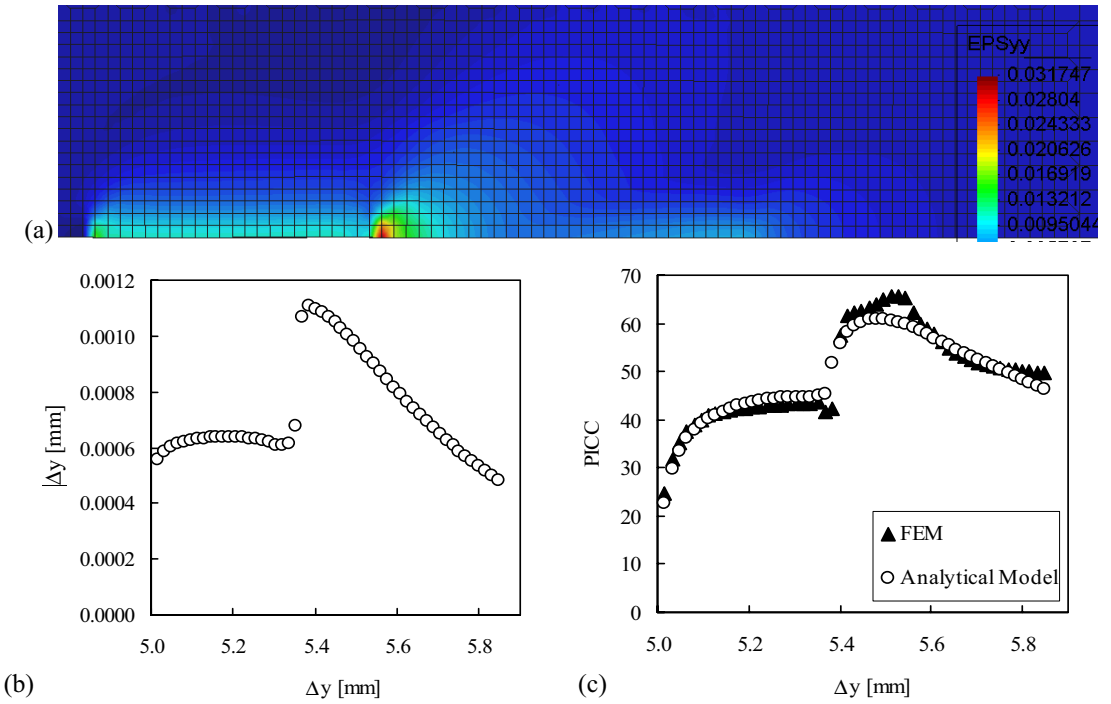

Fig. 9. Overload case (OLR=1.6; baseline: F_{min}= 0, F_{max}=140 N). (a) Vertical strain field (ε_{yy}). (b) Δy vs. x-coordinate. (c) PICC vs. x-coordinate.

- the linear superposition effect applies to the effect of the individual plastic wedges on PICC;
- the surface value of plastic strain isn't representative of the all plastic wedge and a global value is required. The integration of ε_{yy} versus y curve, which was called Δy, was considered. Δy was found adequate to characterize the effects of load level and crack propagation on the residual plastic field;
- the influence of individual plastic wedges on PICC exponentially decreases with the distance to the crack tip, d;
- an empirical model was developed relating the PICC level of an individual plastic wedge, with its distance to crack tip, d, and with the plastic deformation level, Δy. The model was validated and is quite interesting to predict PICC only from residual plastic field and to isolate the effect of residual plastic wedges, from other phenomena, like discontinuous closure or crack tip blunting.

References

[1] Ritchie RO, Suresh S, Moss CM. Near-threshold fatigue crack growth in 2(1/4)Cr-1 Mo pressure vessel steel in air and hydrogen. *J Eng Mater Technol-Trans ASME* 1980;**102**:293–9.

[2] Suresh S, Ritchie RO. On the influence of fatigue underloads on cyclic crack growth at low stress intensities. *Mater Sci Eng* 1981;**51**:61–69.

[3] Suresh S, Ritchie RO. A geometric model for fatigue crack closure induced by fracture surface morphology. *Metall Trans A* 1982;**13**:1627–31.

[4] Elber W. The significance of fatigue crack closure under cyclic tension. In: *Damage Tolerance in Aircraft Structures, ASTM STP 486*. Philadelphia: American Society for Testing and Materials; 1971, p.230–42.

[5] Blom AF, Holm DK. An experimental and numerical study of crack closure. *Eng Fract Mech* 1984;**22**:997–1011.

[6] Borrego LP, Ferreira JM, Costa JM. Fatigue crack growth and crack closure in an AlMgSi alloy. *Fatigue Fract Engng Mater Struct* 2001;**24**:255–65.

[7] Bao H, McEvily AJ. On plane stress-plane strain interactions in fatigue crack growth. *Int J Fatigue* 1998;**20**:441–8.

[8] Costa JDM, Ferreira JAM. Effect of stress ratio and specimen thickness on fatigue crack growth of CK45 steel. *Theor Appl Fract Mech* 1998;**30**:65–73.

[9] Elber W. Fatigue crack closure under cyclic tension. *Eng Fract Mech* 1970;**2**:37–45.

[10] Solanki K, Daniewicz SR, Newman JR. JC. Finite element analysis of plasticity-induced crack closure: an overview. *Eng Fract Mech* 2004;**71**:149–71.

[11] McClung RC, Sehitoglu H. On the finite element analysis of fatigue crack closure-1: Basic modelling issues. *Eng Fract Mech* 1989;**33**:237–252.

[12] González-Herrera A, Zapatero J. Influence of minimum element size to determine crack closure stress by the finite element method. Eng Fract Mech 2005;**72**:337–55.

[13] Pommier S, Freitas M. Effect on fatigue crack growth of interactions between overloads. *Fatigue Fract Engng Mater Struct* 2002;**25**:709–22.

[14] Branco R, Rodrigues DM, Antunes FV. Influence of through-thickness crack shape on plasticity induced crack closure. *Fatigue Fract Engng Mater Struct* 2008;**31**:209–20.

[15] Rodrigues DM, Antunes FV. Finite element simulation of plasticity induced crack closure with different material constitutive models. *Eng Fract Mech* 2009;**76**:1215–30.

[16] Solanki K, Daniewicz SR, Newman Jr. JC. Finite element modelling of plasticity-induced crack closure with emphasis on geometry and mesh refinement effects. *Eng Fract Mech* 2003;**70**:1475–89.

[17] Roychowdhury S, Dodds Jr. RH. A numerical investigation of 3-D small-scale yielding fatigue crack growth. *Eng Fract Mech* 2003;**70**:2363–83.

[18] Wu J, Ellyin F. A study of fatigue crack closure by elastic-plastic finite element analysis for constant-amplitude loading. *Int J Fract* 1996;**82**:43–65.

[19] Parks S-J, Earmme Y-Y, Song J-H. Determination of the most appropriate mesh size for a 2-D finite element analysis of fatigue crack closure behaviour. *Fatigue Fract Engng Mater Struct* 1997;**20**:533–45.

[20] Antunes FV, Borrego LFP, Costa JD, Ferreira JM. A numerical study of fatigue crack closure induced by plasticity. *Fatigue Fract Engng Mater Struct* 2004;**27**:825–36.

[21] Jiang Y, Feng M, Ding F. A re-examination of plasticity-induced crack closure in fatigue crack propagation. *Int J Plast* 2005;**21**:1720–40.

[22] Parry MR, Syngellakis S, Sinclair I. Numerical modeling of combined roughness and plasticity induced crack closure effects in fatigue. *Mater Sci Eng A* 2000;**291**:224–34.

[23] Lee HJ, Song JH. Finite element analysis of fatigue crack closure under plane strain conditions: stabilization behaviour and mesh size effect. *Fatigue Fract Engng Mater Struct* 2005;**28**:333–42.

[24] Kim J-S, Kang JY, Song J-H. Elucidation of fatigue crack closure behaviour in surface crack by 3-D finite element analysis. *Int J Fatigue* 2007;**29**:168–80.

[25] Chaparro BM, Thuillier S, Menezes LF, Manach PY, Fernandes JV. Material parameters identification: Gradient-based, genetic and hybrid optimization algorithms. *Comp Mater Sci* 2008;**44**:339–46.

[26] Menezes LF, Teodosiu C. Three-dimensional numerical simulation of the deep-drawing process using solid finite elements. *J Mater Process Technol* 2000;**97**:100–6.

[27] Oliveira MC, Alves JL, Menezes LF. Improvement of a frictional contact algorithm for strongly curved contact problems. *Int J Numer Methods Eng* 2003;**58**:2083–101.

[28] Oliveira MC, Alves JL, Chaparro BM, Menezes LF. Study on the influence of work-hardening modeling in spring-back prediction. *Int J Plast* 2007;**23**:516–43.

[29] Alves JL, Menezes LF. Application of tri-linear and tri-quadratic 3-D solid FE in sheet metal forming process simulation. In: K. Mori, editor. *NUMIFORM 2001*, Japan, 2001; p. 639–44.

[30] Oliveira MC, Menezes LF. Automatic correction of the time step in implicit simulations of the stamping process. *Finite Elem Anal Des* 2004;**40**:1995–2010.

[31] Antunes FV, Rodrigues D. Numerical simulation of plasticity induced crack closure: identification and discussion of parameters. *Eng Fract Mech* 2008;**75**:3101–20.